




# Exploring Magnitude Estimation for Earthquake Early Warning Using Available P-Wave Time Windows Based on Chinese Strong-Motion Records

YUAN WANG,<sup>1,2</sup> SHANYOU LI,<sup>1,2</sup> and JINDONG SONG<sup>1,2</sup> 

**Abstract**—Quickly determining earthquake size by extracting information after P-wave arrival is a critical issue for earthquake early warning systems. However, early warning parameters are often calculated using a fixed-length (3–5 s) P-wave time window for rapid magnitude estimation. In this paper, we directly investigate magnitude-scaling relationships within the available P-wave time window (APTW, defined as the window period starting from the trigger time of the P wave and ending at the arrival of the S wave) and explore a new real-time magnitude estimation approach (the APTW method). The results of an offline application demonstrate the good performance of the APTW method in terms of the stability of magnitude estimation for small to moderate earthquakes and improved estimation for large earthquakes. The APTW method can provide estimates earlier, and the estimated magnitudes are more stable. The proposed method of establishing magnitude relationships could provide an alternative choice for magnitude estimation in earthquake early warning systems.

**Keywords:** Earthquake early warning, P waves, magnitude estimation, P-wave time window.

## 1. Introduction

Earthquake early warning systems (EEWSs) can monitor an area in real time and quickly detect an occurring earthquake. Within a few seconds of earthquake occurrence, EEWSs can rapidly predict the ground shaking and warn the target area prior to

the arrival of the destructive wave. EEWSs have been established or are being tested in more and more countries and regions worldwide to reduce seismic risk (Allen & Melgar, 2019). On-site warning, the common concept used in existing EEWSs, detects the initial P-wave information at single stations and predicts the peak shaking at the same site, i.e., the Urgent Earthquake Detection and Alarms System (UrEDAS) used along the rail systems in Japan (Nakamura & Saita, 2007) and the  $\tau_c$ -Pd method (Wu & Kanamori, 2005a, 2005b) tested in California (Böse et al., 2009) and Taiwan (Hsiao et al., 2009; Hsu et al., 2018; Wu et al., 2018). Regional EEWSs use early information concerning the seismic waves obtained from the seismic network located near the source area and predict the ground shaking after analyzing data from multiple stations, e.g., the Seismic Alert System of Mexico (Espinosa-Aranda et al., 2009), the operational warning system implemented by the Japan Meteorological Agency (Kamigaichi et al., 2009), the EEWS of Taiwan developed by the Central Weather Bureau using the national seismic network (Wu et al., 2013), the Virtual Seismologist methodology and ElarmS EEW methodology tested in California (Allen, Brown, et al., 2009, b; Cua et al., 2009), the probabilistic evolutionary approach (PRESTo) tested in southern Italy (Iannaccone et al., 2010), and the warning systems for Bucharest, Romania (Böse et al., 2007) and Istanbul, Turkey (Alcik et al., 2009).

As a result of the long-term mutual pushing forces of the Pacific and Indian plates, China experiences strong seismic activity. Since 2000, China has conducted systematic research on earthquake early warning technologies and has developed related technologies such as earthquake location, magnitude

---

**Electronic supplementary material** The online version of this article (<https://doi.org/10.1007/s00024-022-03062-4>) contains supplementary material, which is available to authorized users.

---

<sup>1</sup> Key Laboratory of Earthquake Engineering and Engineering Vibration, Institute of Engineering Mechanics, China Earthquake Administration, Harbin, People's Republic of China. E-mail: wangyuanseis@gmail.com; shanyou@iem.ac.cn; jdsong@iem.ac.cn

<sup>2</sup> Key Laboratory of Earthquake Disaster Mitigation, Ministry of Emergency Management, No. 29 Xuefu Road, Harbin 150080, People's Republic of China.

estimation, and intensity prediction. In November 2010, the China Earthquake Administration launched a national project for Seismic Intensity Rapid Reporting (SIRR) and EEWS. Currently, the preliminary design report for the project has been approved by the National Development and Reform Commission and the project has moved to the implementation stage. EEWSs were deployed in the Beijing capital region (Peng et al., 2011), Fujian region (Zhang et al., 2016), and other regions of China (Peng et al., 2020) for online performance testing. With the implementation of the SIRR and EEWS national project, the observation capabilities of the existing seismic network are gradually being strengthened.

Quickly providing robust estimations of earthquake magnitude is a critical issue for EEWSs. Previous studies have typically used information from the initial P wave to extract parameters related to the magnitude and have provided estimates based on established scaling relationships for the selected datasets. The absolute peak values of the displacement ( $P_d$ ) and velocity ( $P_v$ ) are commonly used amplitude parameters for magnitude estimation (Wu & Kanamori, 2005a, 2005b; Zollo et al., 2006). Period parameters, such as the characteristic  $\tau_c$  (Kanamori, 2005) and predominant  $\tau_p^{\max}$  (Allen & Kanamori, 2003) period parameters use the frequency content of the P wave to make a rapid estimation of earthquake magnitude. In addition, Festa et al. (2008) proposed the integral of the velocity squared (IV2), which is a parameter directly related to the energy released in the first few seconds of an earthquake and can be applied to earthquake magnitude estimation.

These early warning parameters are often calculated in a fixed-length P-wave time window (2–4 s) for rapid magnitude estimation. For large earthquakes, the relevant complex rupture processes may not be completed in such a short time window, leading to underestimations of the magnitude (Colombelli et al., 2012; Lomax & Michelini, 2009). To overcome this well-known saturation problem, other studies have proposed the use of extended P-wave time windows. Chen et al. (2017) proposed a less-saturated approach to update the magnitude estimation by extending the time window and establishing a regression relation between the peak

displacement and the magnitude at each time step (1- to 10-s time interval). However, extending the P-wave time window in a uniform way for all stations will induce S-wave contamination for the near-source stations, leading to overestimation of the magnitude in the early stage of an earthquake. Colombelli and Zollo (2015) focused on the time evolution of the logarithm of P-wave peak displacement (LPDT) for source characterization and found that magnitude can be estimated quite accurately when the LPDT curve reaches a plateau (Wang et al., 2021). The plateau of the LPDT curve can be simply regarded as capturing the peak value of the displacement within a pure P-wave time window.

In this study, we directly investigate the relationships between the early warning (amplitude-, frequency- and energy-based) parameters under the available P-wave time windows (APTW, defined as the window period starting from the trigger time of the P wave until the arrival of the S wave) and magnitude. We also explore a parameter combination method for magnitude estimation based on the characteristics of the established relationships. Based on the analysis of small to large earthquakes, we then discuss the behavior of the proposed approach and possible improvements for future applications.

## 2. Data

We used a strong-motion dataset of events recorded for the period 2007–2015 provided by the China Strong-Motion Network Centre, China Earthquake Administration. The catalog magnitudes of all the analyzed events in this dataset are given in surface magnitude ( $M_s$ ), which is denoted as  $M$  in this study. For (1) aiming at earthquakes that may cause damage, (2) maximizing the use of near-source stations, and (3) reducing scattering caused by site or source effects by averaging the various stations (Peng et al., 2014), we chose the corresponding criteria: (1)  $M \geq 4$ ; (2) epicentral distances  $< 120$  km; and (3) each earthquake having at least three records. Accordingly, we selected 87 earthquakes with 1265 three-component seismic records for this study. Figure 1 shows the epicenters of the selected events and the locations of the stations in China, of which two

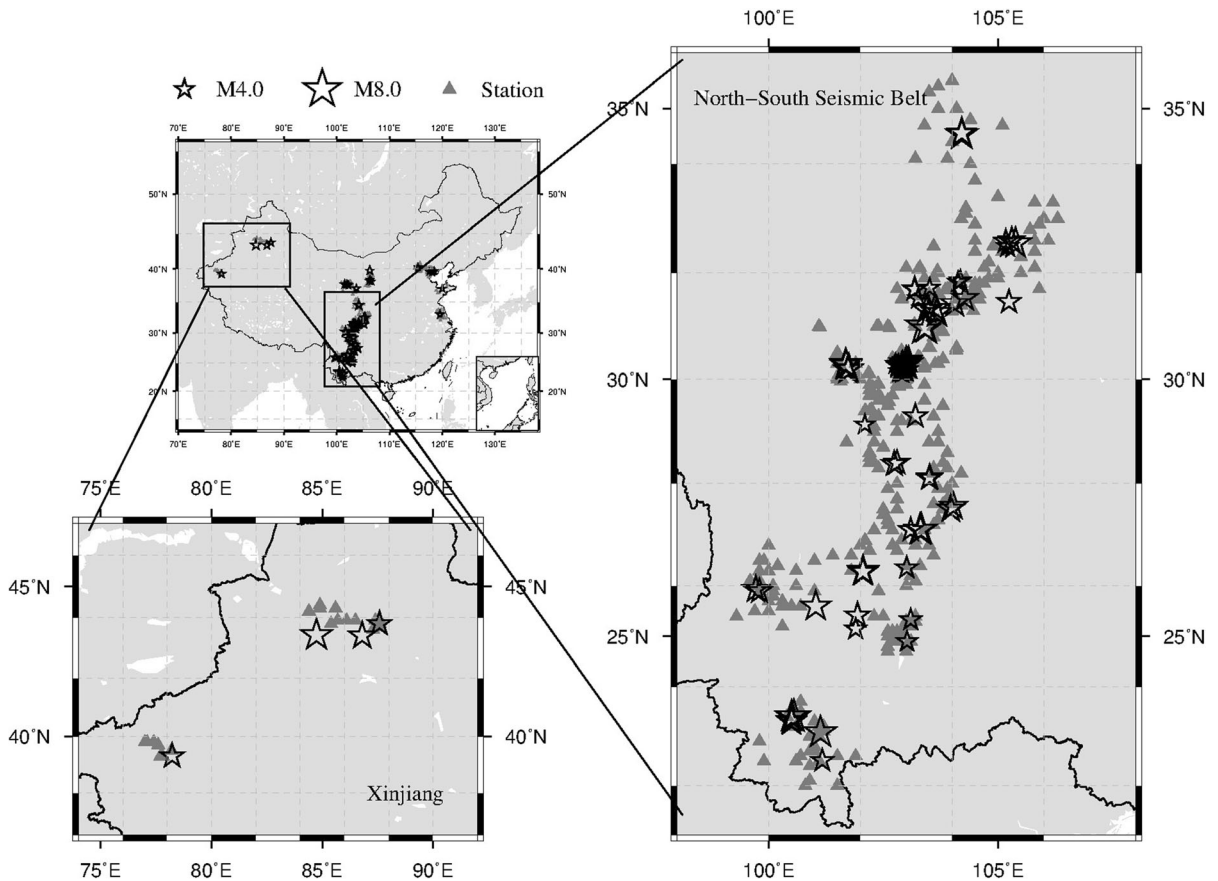


Figure 1  
Distribution of the analyzed earthquakes (stars) and stations (triangles)

main seismic regions (the North–South Seismic Belt and the Xinjiang region) have been enlarged. Figure 2 shows the histogram distributions of the analyzed records as a function of magnitude and epicentral distance.

To identify the onset of the P wave, we used the short-term/long-term average method for automatic picking (Allen, 1978, 1982) and then manually picked the P-wave arrival for corrections. The acceleration records were integrated once to velocity and twice to displacement. To remove the low-frequency drift caused by integration, we applied a high-pass Butterworth filter with a cut-off frequency of 0.075 Hz to the integrated displacement.

### 3. Method

To determine the length of the APTW, we chose four stations with a clear seismic phase randomly in every 20-km distance bin from the dataset and picked the S-wave arrival time of the selected records manually. We computed the interval between the arrivals of the P and S waves using the following relationship:

$$T_s - T_p = b \cdot R, \quad (1)$$

where  $T_p$  is the P-wave onset time,  $T_s$  is the arrival time of the S wave,  $R$  is the hypocentral distance in kilometers, and  $b = 0.13$  s/km, as derived via linear regression after manually picking the S-wave arrival times of the selected records. Supplementary Fig. S1 shows the data distribution and the best-fit curve of

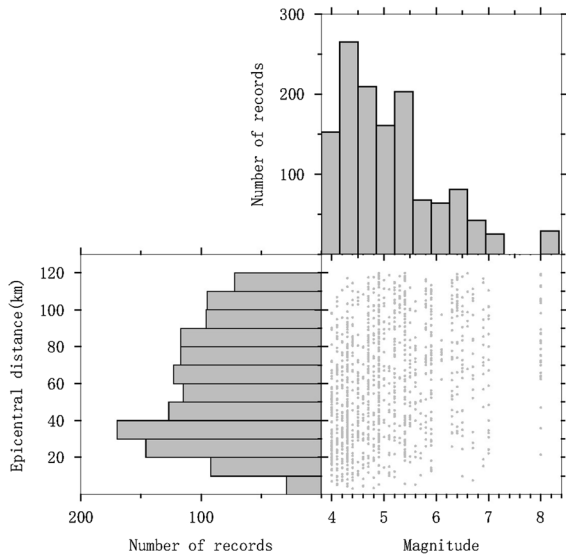


Figure 2

Distribution of the analyzed records as a function of epicentral distance and magnitude

Eq. (1). Considering its variability along the entire distance range, we set the length of the APTW to be 80% of  $(T_s - T_p)$  to minimize the possibility of introducing S waves.

The definitions of the analyzed parameters are illustrated in Fig. 3. In the following sections, we describe the specific processing steps for the computation for each parameter and the results for the relationships between magnitude and the parameters calculated in the APTWs.

### 3.1. Magnitude-Scaling Relationship

#### 3.1.1 Peak displacement ( $P_d$ )

Wu and Zhao (2006) found the empirical attenuation relationship among the peak displacement ( $P_d$ ), the hypocentral distance ( $R$ ) and the magnitude ( $M$ ):

$$\log_{10}(P_d) = AM + B\log_{10}(R) + C. \quad (2)$$

In this study, we measured  $P_d$  from the vertical component of each filtered displacement in the APTWs and obtained the best-fit relationship via least-squared regression:

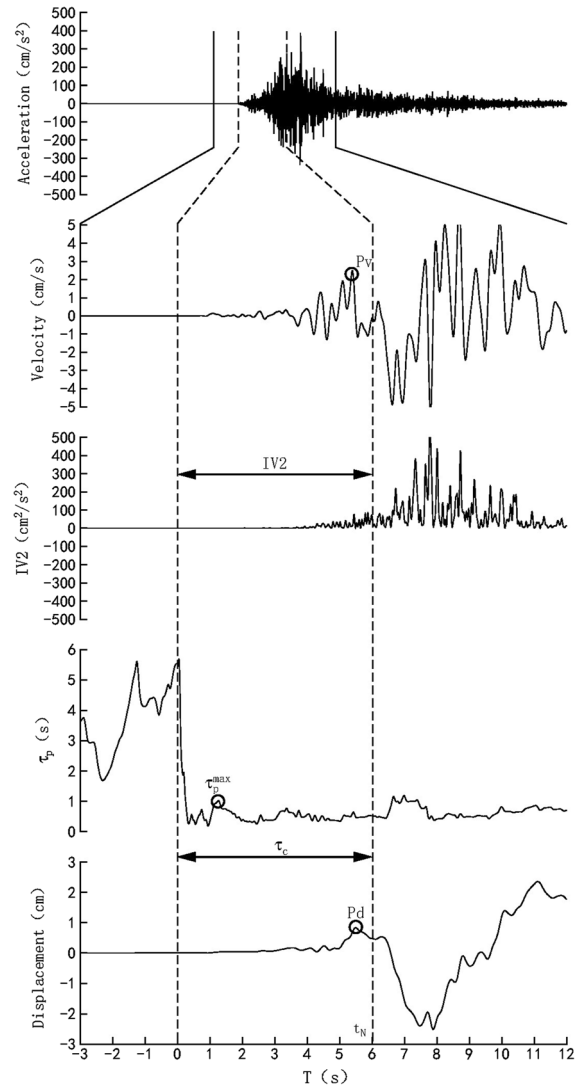


Figure 3

Example showing the peak displacement ( $P_d$ ), peak velocity ( $P_v$ ), integral of the squared velocity (IV2), predominant period ( $\tau_p^{\max}$ ), and characteristic period ( $\tau_c$ ). The dashed line represents the length of the available-P-wave time window (APTW)

$$\begin{aligned} \log_{10}(P_d) &= 0.559(0.021)M - 0.897(0.081)\log_{10}(R) \\ &\quad - 3.351(0.149) \text{ RMSE} \\ &= 0.330. \end{aligned}$$

(3)

The quantities in parentheses represent the 95% confidence intervals for the coefficient estimate; for instance, the 95% confidence interval for the  $A$  coefficient is  $[0.559 - 0.021, 0.559 + 0.021]$ . The root mean square error (RMSE) represents the

deviation between the observed value and the predicted value. Following the approach of Zollo et al. (2006), we normalized the  $P_d$  value to 10 km ( $P_d^{10\text{km}}$ ) to derive the magnitude dependence of the P-wave amplitude. Linear fitting of the event-averaged  $P_d^{10\text{km}}$  value and the magnitude yielded the best-fit regression:

$$\begin{aligned}\log_{10}(P_d^{10\text{km}}) &= 0.583(0.040)M \\ &\quad - 4.354(0.204) \text{ RMSE} \\ &= 0.160.\end{aligned}\quad (4)$$

To estimate magnitude with the observed  $P_d$  value, we recalibrated the relationship according to the equation ( $M = k\log_{10}(P_d^{10\text{km}}) + b$ ):

$$\begin{aligned}M &= 1.56(0.106) \log_{10}(P_d^{10\text{km}}) \\ &\quad + 7.25(0.157) \text{ RMSE} \\ &= 0.262.\end{aligned}\quad (5)$$

The logarithm of the  $P_d^{10\text{km}}$  value calculated in the APTWs as a function of magnitude is shown in Fig. 4a. The event-averaged  $P_d^{10\text{km}}$  values are concentrated on the fitted line with small deviations. Compared with the results found when using a fixed P-wave time window (PTW) of 3 s, as shown in Fig. 4b, the relationship derived from the APTWs has

a smaller RMSE and a larger slope. More importantly, the measurements for the  $M$  8 event, which are lower than the expected value, are greatly improved when applying the APTWs.

### 3.1.2 Peak velocity ( $P_v$ )

The peak velocity ( $P_v$ ) was measured from the vertical component of the velocity in the APTWs without applying any high-pass filters. Following a similar attenuation relationship to that of Eq. (2), we derived the best-fit relationship for  $P_v$ :

$$\begin{aligned}\log_{10}(P_v) &= 0.397(0.021)M \\ &\quad - 1.143(0.083) \log_{10}(R) \\ &\quad - 0.997(0.152) \text{ RMSE} \\ &= 0.337.\end{aligned}\quad (6)$$

After normalizing the  $P_v$  measurements to 10 km ( $P_v^{10\text{km}}$ ), we obtained the best-fit relationship between the event-averaged  $P_v^{10\text{km}}$  and the magnitude:

$$\begin{aligned}\log_{10}(P_v^{10\text{km}}) &= 0.411(0.043)M \\ &\quad - 2.193(0.221) \text{ RMSE} \\ &= 0.174.\end{aligned}\quad (7)$$

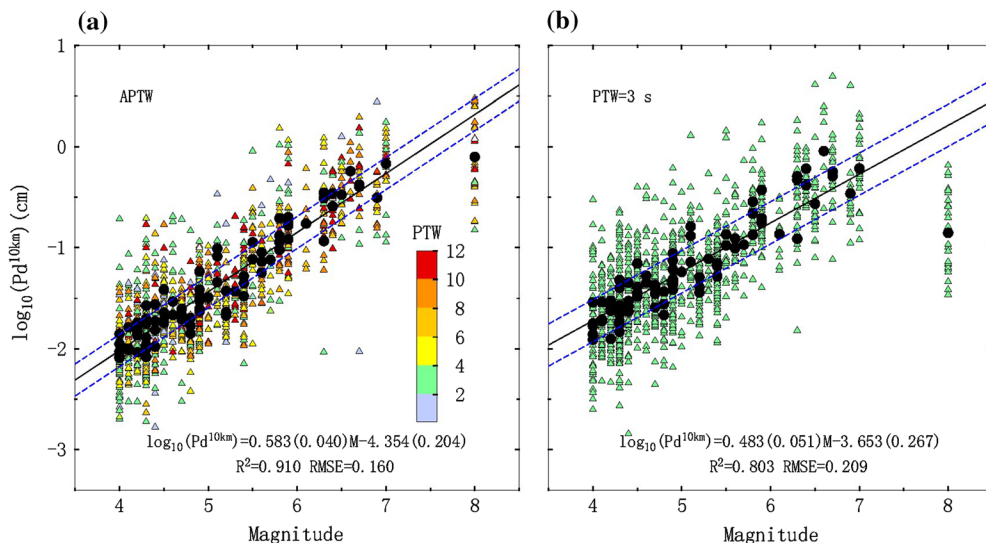


Figure 4

The magnitude relationship of the  $P_d^{10\text{km}}$  calculated in **a** APTWs and **b** a fixed PTW of 3 s. Triangles with color scale and black circles stand for single  $P_d^{10\text{km}}$  values for different lengths of PTW and event-averaged  $P_d^{10\text{km}}$  value, respectively. The solid line represents the relation derived in this study



Similarly to Eq. (5), the magnitude estimate is given by

$$\begin{aligned} M &= 1.973(0.206) \log_{10}(P_v^{10\text{km}}) \\ &\quad + 5.29(0.084) \text{ RMSE} \\ &= 0.381. \end{aligned} \quad (8)$$

As Fig. 5a shows, the event-averaged  $P_v^{10\text{km}}$  values calculated using the APTWs are proportional to the magnitude over the entire magnitude range. Compared with the results of using a fixed 3-s PTW, shown in Fig. 5b, the magnitude relationship using the APTWs shows a higher correlation with magnitude without showing any saturation effect for the largest  $M$  8 event.

### 3.1.3 Integral of the velocity squared (IV2)

Festa et al. (2008) proposed the integral of the squared velocity (IV2), which is related to the energy released by earthquakes, for estimating the earthquake magnitude in real time:

$$\text{IV2} = \int_t^{t+\Delta t} v^2(t) dt, \quad (9)$$

where  $t$  is the first P-wave arrival and  $v$  is the

modulus of the velocity squared evaluated using the three velocity components. Following the same processing steps as in Festa et al. (2008), we applied a band-pass filter with a frequency band of 0.05–10 Hz for the integrated velocity, the difference being that, here, the time length of the signal ( $\Delta t$ ) is set to the APTW. By calculating the IV2 value and normalizing it to 10 km ( $\text{IV2}^{10\text{km}}$ ), we obtained the best-fit attenuation relationship of IV2 and the relationship of the magnitude dependence of  $\text{IV2}^{10\text{km}}$ :

$$\begin{aligned} \log_{10}(\text{IV2}) &= 0.874(0.044)M \\ &\quad - 1.340(0.171) \log_{10}(R) \\ &\quad - 4.212(0.314) \text{ RMSE} \\ &= 0.695, \end{aligned} \quad (10)$$

$$\begin{aligned} \log_{10}(\text{IV2}^{10\text{km}}) &= 0.926(0.086)M \\ &\quad - 5.768(0.440) \text{ RMSE} \\ &= 0.346. \end{aligned} \quad (11)$$

The magnitude estimate is given by

$$\begin{aligned} M &= 0.913(0.085) \log_{10}(\text{IV2}^{10\text{km}}) \\ &\quad + 6.051(0.116) \text{ RMSE} \\ &= 0.344. \end{aligned} \quad (12)$$

A comparison between the magnitude relationships for  $\text{IV2}^{10\text{km}}$  measured using the APTWs and

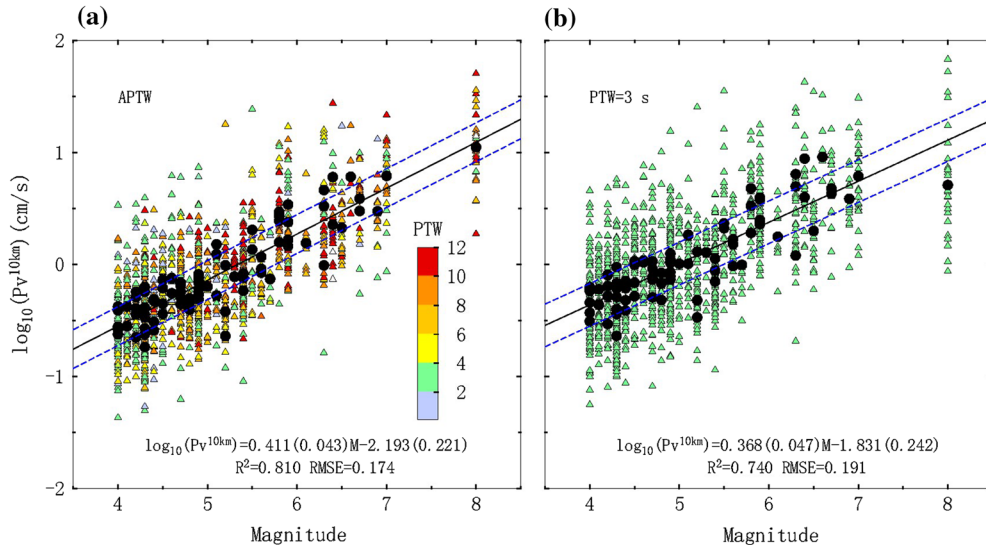


Figure 5

The magnitude relationship of the  $P_v^{10\text{km}}$  calculated in **a** APTWs and **b** a fixed PTW of 3 s. Triangles with color scale and black circles stand for single  $P_v^{10\text{km}}$  values for different lengths of PTW and event-averaged  $P_v^{10\text{km}}$  value, respectively. The solid line represents the relation derived in this study

those measured using a fixed 3-s PTW is shown in Fig. 6. Some near-source stations with the fixed 3-s PTW, which may be affected by contamination from S waves, produced large  $IV2^{10km}$  values, whereas the scattering in the distribution of  $IV2^{10km}$  measurements was reduced when applying the APTWs. A higher correlation coefficient and a smaller RMSE can be found in the relationship derived after applying the APTWs. Moreover, almost all the event-averaged values ( $IV2^{10km}$ ) calculated using the APTWs are distributed around the best-fit line, and a smaller saturation effect can be found for the  $M$  8 event.

### 3.1.4 Predominant period $\tau_p^{max}$

Allen and Kanamori (2003) defined  $\tau_p^{max}$  as the maximum value of the  $\tau_p(t)$  data in a given duration following P-wave onset. The  $\tau_p(t)$  function was given by Nakamura (1988):

$$\tau_i^p = 2\pi\sqrt{X_i/D_i}, \quad (13)$$

$$X_i = \alpha X_{i-1} + x_i^2, \quad (14)$$

$$D_i = \alpha D_{i-1} + (dx/dt)_i^2, \quad (15)$$

where  $x_i$  is the vertical component of the velocity at time  $i$  and  $\alpha$  is a 1 s smoothing constant that is set to 0.95 for a rate of 200 samples per second. We applied a 0.075-Hz high-pass filter to the velocity and computed  $\tau_p^{max}$  in the period from 0.25 s after the P-wave arrival to the end of the APTW (Nazeri et al., 2017).

Figure 7a shows the distribution of  $\tau_p^{max}$  calculated in the APTW as a function of magnitude. Even though the scatter of the individual  $\tau_p^{max}$  values is rather large, the averaged  $\log(\tau_p^{max})$  values of the events are linearly proportional to the magnitude, except for the  $M$  8 event, which has an obviously lower value than expected. The best-fit relationship between the magnitude and the event-averaged  $\tau_p^{max}$  value was then derived via a least-square analysis:

$$\begin{aligned} \log_{10}(\tau_{pmax}) &= 0.239(0.04)M \\ &\quad - 1.532(0.206) \text{ RMSE} \\ &= 0.162. \end{aligned} \quad (16)$$

The magnitude estimate is given by

$$\begin{aligned} M &= 2.607(0.437) \log_{10}(\tau_{pmax}) \\ &\quad + 5.903(0.180) \text{ RMSE} \\ &= 0.536. \end{aligned} \quad (17)$$

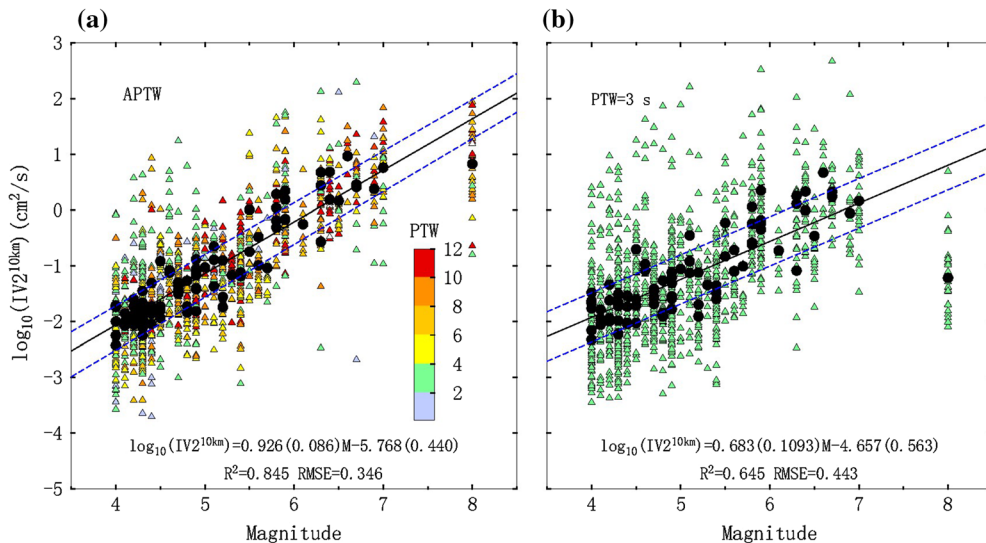


Figure 6

The magnitude relationship of the  $IV2^{10km}$  calculated in **a** APTWs and **b** a fixed PTW of 3 s. Triangles with color scale and black circles stand for single  $IV2^{10km}$  values for different lengths of PTW and event-averaged  $IV2^{10km}$  value, respectively. The solid line represents the relation derived in this study

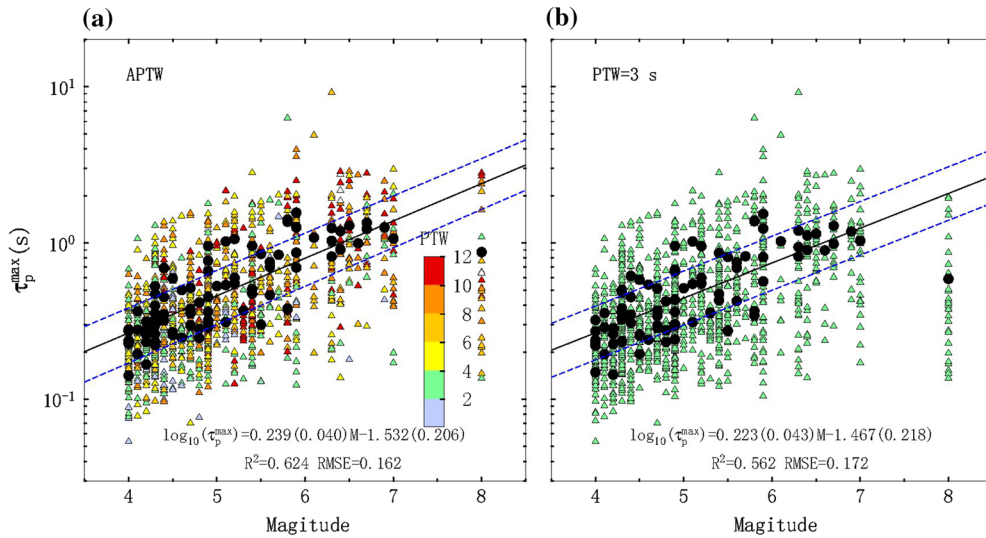


Figure 7

The magnitude relationship of the  $\tau_p^{\max}$  calculated in **a** APTWs and **b** a fixed PTW of 3 s. Triangles with color scale and black circles stand for single  $\tau_p^{\max}$  values for different lengths of PTW and event-averaged  $\tau_p^{\max}$  value, respectively. The solid line represents the relation derived in this study

Examining the distribution of  $\tau_p^{\max}$  calculated using a fixed 3-s PTW, as shown in Fig. 7b, we find that the derived relationships for PTW = 3 s have a similar trend to the results derived using the APTWs, indicating that the  $\tau_p^{\max}$  relationship is not significantly affected by the length of the PTW.

### 3.1.5 Characteristic period $\tau_c$

Kanamori (2005) proposed an averaged period parameter,  $\tau_c$ , to represent the frequency information of the seismic wave; this parameter has been proven to be proportional to the event magnitude. The period parameter  $\tau_c$  was computed using the following equation:

$$\tau_c = \frac{2\pi}{\sqrt{r}}, \quad (18)$$

$$r = \frac{\int_0^{\tau_0} \dot{u}^2(t) dt}{\int_0^{\tau_0} u^2(t) dt}, \quad (19)$$

where  $u(t)$  and  $\dot{u}(t)$  are the vertical displacement and velocity, respectively, and  $\tau_0$  is the duration from the P-wave onset of each record. Here,  $\tau_0$  is set to the APTW, and the integrated velocity and displacement are both filtered using a high-pass filter with a cut-off

frequency of 0.075 Hz to eliminate the effects of the low-frequency drift introduced by the integration.

Because the  $\tau_c$  parameter is sensitive to the signal-to-noise ratio of the data, previous studies have usually set a criterion to remove low signal-to-noise ratio data (Zollo et al., 2010; Ziv, 2014). Following the idea of Zollo et al. (2010), we selected data with  $P_v > 0.05$  cm/s for the calculation of  $\tau_c$  and established the magnitude-scaling relationship for the event-averaged  $\tau_c$  value using the APTW:

$$\log_{10}(\tau_c) = 0.265(0.041)M - 1.461(0.212) \text{ RMSE} = 0.160. \quad (20)$$

The magnitude is estimated such that:

$$M = 2.593(0.398) \log_{10}(\tau_c) + 5.400(0.120) \text{ RMSE} = 0.502. \quad (21)$$

The distribution of the  $\tau_c$  measurements and the derived relationships are shown in Fig. 8. The event-averaged  $\tau_c$  values scale with the magnitude for  $M < 7$ ; however, the  $M 8$  event has a smaller event-averaged  $\tau_c$  than expected. The  $\tau_c$  value calculated with the APTWs has a higher correlation with the



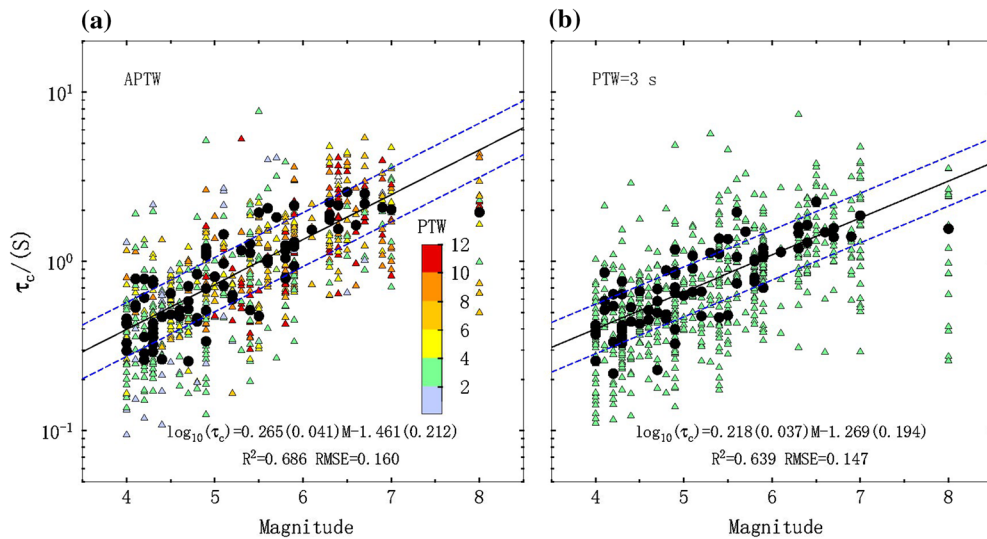


Figure 8

The magnitude relationship of the  $\tau_c$  calculated in **a** APTWs and **b** a fixed PTW of 3 s. Triangles with color scale and black circles stand for single  $\tau_c$  values for different lengths of PTW and event-averaged  $\tau_c$  value, respectively. The solid line represents the relation derived in this study

magnitude, and the derived magnitude with the APTWs produced a higher slope than the relationship of using a fixed 3-s PTW.

### 3.2. Parameter Combination for Magnitude Estimation

On the basis of the magnitude-scaling relationships described above, here we summarize the characteristics of early warning parameters using APTWs for magnitude estimation. The amplitude parameters ( $P_d$  and  $P_v$ ) have a higher correlation with the earthquake magnitude after applying the APTWs. The magnitude prediction equation of  $P_d$  (Eq. (5)) has the smallest RMSE (0.262 magnitude units) of all the parameters. Even though  $P_v$  shows a larger magnitude estimation error (0.381 magnitude units, Eq. 8) than  $P_d$ ,  $P_v$  has the advantage of accurately estimating large earthquakes without any underestimation. Using APTWs, the energy-based parameter  $IV2^{10km}$  was significantly improved (the coefficient of determination increased from 0.645 to 0.845); however, the  $M 8$  event was still underestimated. As for the period-based parameters ( $\tau_p^{max}$  and  $\tau_c$ ), their magnitude-scaling relationships show larger scatter than those of the other parameters, and the correlation

between the period-based parameters and the magnitude was less affected by the PTW.

Therefore, considering the underestimation of  $IV2^{10km}$  for large earthquakes and the scatter of the single period-based parameters, we explored a real-time approach that integrates the use of  $P_d$  (the highest correlation with magnitude) and  $P_v$  (good performance in predicting large events) using APTWs to estimate the magnitude; that is, once the earthquake occurs, the method begins to calculate the  $P_d^{10km}$  and  $P_v^{10km}$  values of all the available stations whose time window length has reached the APTW and averages the magnitude estimates based on Eqs. (5) and (8) to obtain a real-time prediction curve of earthquake magnitude as follows:

$$M_{(t)} = \frac{\text{Mean}(M_{P_d10km(t)}) + \text{Mean}(M_{P_v10km(t)})}{2}, \tag{22}$$

where  $M_{P_d10km(t)}$  and  $M_{P_v10km(t)}$  are the magnitude estimates of all the available stations using the APTWs with  $P_d^{10km}$  and  $P_v^{10km}$ , respectively.

#### 4. Offline Applications

Because the length of the APTW is related to the hypocentral distance of the triggered station, the time windows of near-source stations (e.g., hypocentral distance < 30 km) may be shorter than 3 s, and the far stations may require additional time to reach the APTW. Therefore, to evaluate whether our method underestimates small to moderate earthquakes ( $M \leq 7$ ) in the early stage and whether it takes more time to achieve good results for large earthquakes, we applied our method to all the earthquakes in the dataset to show the performance in terms of the stability of the magnitude estimation of small to moderate earthquakes and the improvement and timeliness with respect to estimating the magnitude of large earthquakes.

Once a station is triggered, the estimation of the magnitude is provided only when the length of the time window has reached the APTW. The time required for each station is the sum of the P-wave propagation time and the required length of the APTW. With more stations joining the computation, the magnitude estimation is constantly updated by averaging the estimated values of all the available stations. For comparison, the results of using  $P_d$  with a fixed 3-s PTW (referred to as the Pd3s method) are also shown.

##### 4.1. Stability When Estimating Small to Moderate Earthquakes

Figure 9 shows how the estimated real-time magnitude error changes with increasing numbers of triggered stations when our method is applied to the events ( $M \leq 7$ ). At the initial stage of the earthquakes (1–2 triggered stations), the magnitude estimation errors for the APTW and Pd3s methods both have large deviations; then the errors of both show a tendency to gradually approach zero as the number of triggered stations continues to increase. To clearly display the performance of the methods in the early stage, a distribution histogram of the magnitude estimation errors when applying the two methods and when only the first three stations are triggered is shown in Fig. 9b. As shown in the figure, 38% of the magnitude estimation errors are within  $\pm 0.5$  and

73% are within  $\pm 1$  for the Pd3s method, while 63% of the magnitude estimation errors are within  $\pm 0.5$  and 91% are within  $\pm 1$  when applying the APTW method. The APTW method can be shown to not cause instabilities in the magnitude estimation associated with the use of a shorter time window. However, the accuracy is significantly improved relative to the Pd3s method (increasing from 38 to 63%) within the  $\pm 0.5$  range of the magnitude estimation error after applying the APTW method. In addition, the estimation error of the APTW method is mostly distributed around +0.25, while the real-time magnitude estimation result of the Pd3s method is distributed around +0.5. This indicates that the fixed 3-s time window for near-source stations may include S waves, leading to a certain degree of magnitude overestimation; conversely the APTW method avoids introducing S waves and reduces the magnitude overestimation caused by near-source stations.

The timeliness of the release of early warning information is often affected by the station spacing and the trigger times of the near-source stations. Therefore, we also plotted time [s] from the event origin time versus the magnitude estimation errors (Fig. 10). The change in the standard deviation of the absolute value of the magnitude estimation error and the average absolute value of the magnitude estimation error in the time interval 5–20 s after the earthquake occurred are shown in Fig. 10b, c, respectively. Because the APTW method requires a shorter time window in the near field ( $R < 30$  km), it can obtain a magnitude estimate faster than the Pd3s method. Figure 10c shows that the average error of the magnitude estimation for the Pd3s method is 1.20 magnitude units 5 s after the occurrence of an earthquake (for comparison, the average error of the magnitude estimation for the APTW method is 0.61 magnitude units). The APTW method obviously has higher accuracy compared with the Pd3s method at the early stage of an earthquake. As time increases, the average magnitude estimation error when applying both methods gradually and steadily decreases, with the two methods having nearly the same error approximately 10 s after the earthquake occurrence.

Figure 11 shows real-time estimation results when applying both methods to the April 20, 2013,

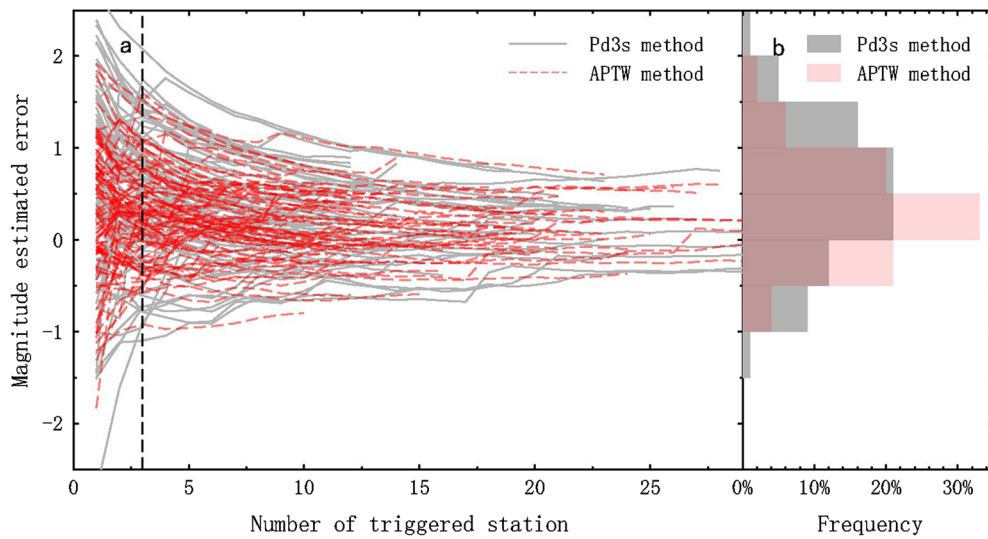


Figure 9

**a** The magnitude estimated error changes with the increasing triggered stations. The red dashed line and solid gray line represent the results obtained by APTW method and Pd3s method, respectively. **b** The distribution histogram of the magnitude estimation errors by applying two methods when the first 3 stations are triggered. The gray area and the light red area represent the estimation result of Pd3s method and APTW method, respectively

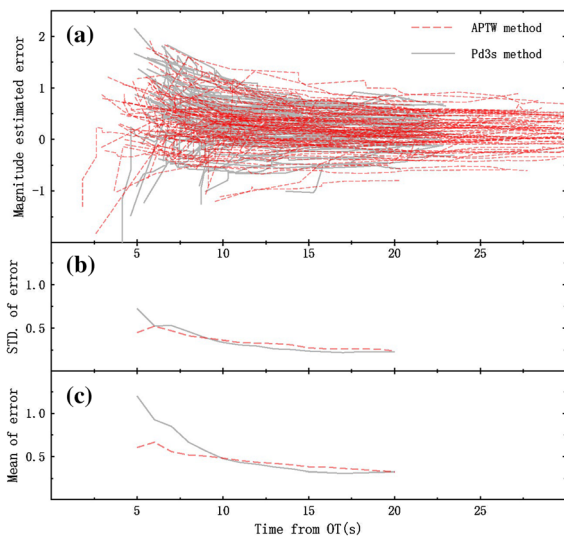


Figure 10

Plots of time (s) from the event origin time (OT) vs. **a** The magnitude estimated error, **b** the standard deviation of the magnitude estimated error, **c** the mean value of the magnitude estimated error. The red dashed line and solid gray line represent the results obtained by APTW method and Pd3s method, respectively

$M_s$  7.0 Lushan earthquake. Both methods provide a magnitude estimate close to the catalog magnitude (dashed line) 9 s after the earthquake occurred and

maintain a stable estimate with the addition of subsequent stations. The two methods differ in performance: the Pd3s method overestimates the magnitude (by 0.53 magnitude units) when the closest two stations are triggered, whereas the APTW method provides a first magnitude estimate (6.8) close to the catalog magnitude, 0.5 s earlier than the first result of the Pd3s method.

#### 4.2. Improvement in and Timeliness of Estimation of Large Earthquakes

To demonstrate the performance of the APTW method when predicting large earthquakes, the time evolutions of the magnitude estimations obtained by applying the APTW and Pd3s methods to the May 12, 2008,  $M_s$  8.0 Wenchuan earthquake are given in Fig. 12. As shown in Fig. 12b, the Pd3s method obtained the first estimated magnitude of 6.8 approximately 7.3 s after the earthquake occurred. With just the first three stations triggered (11.1 s after earthquake occurrence), the magnitude estimate stabilized at 6.4; however, because of the addition of distant stations and the insufficient time window, the magnitude estimate gradually decreased. At 20 s after the

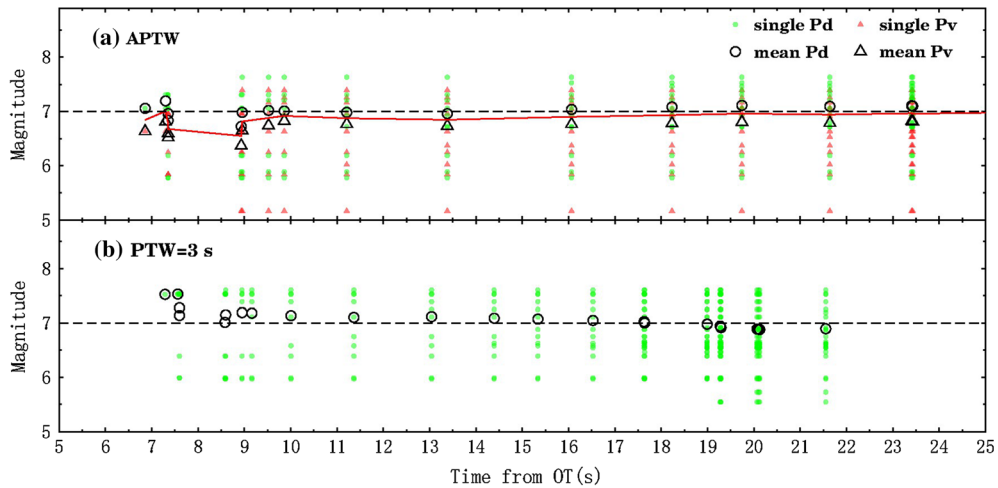


Figure 11

Plots of time (s) from the event origin time vs. the magnitude estimated results of the 2013/04/20 Ms 7.0 Lushan earthquake obtained by **a** APTW method and **b** the Pd3s method. The light green circles and red triangles represent the results obtained by single  $P_d$  and  $P_v$ , respectively. The black circles and triangles represent the magnitude estimates using  $P_d$  and  $P_v$  by averaging all the available stations, respectively. The dashed line represents the catalog magnitude

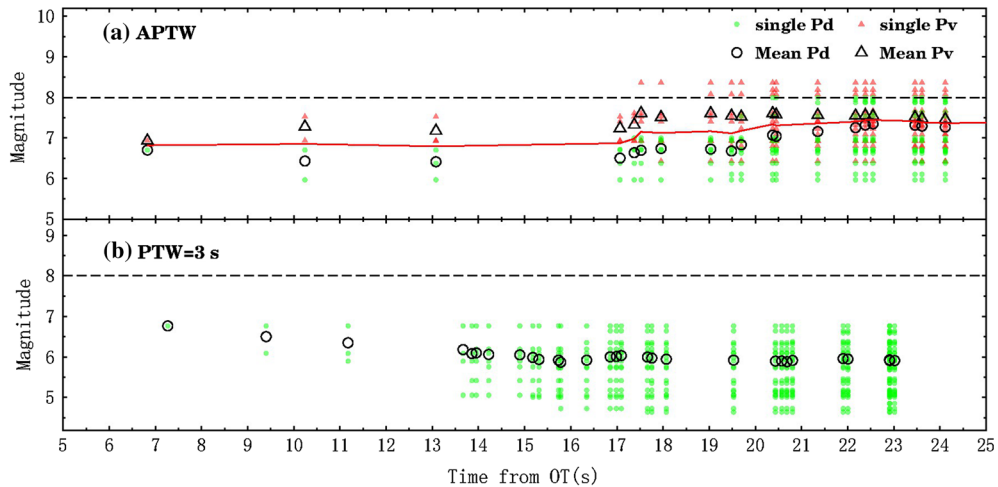


Figure 12

Plots of time (s) from the event origin time vs. the magnitude estimated results of the 2008/05/12 Ms 8.0 Wenchuan earthquake obtained by **a** APTW method and **b** the Pd3s method. The light green circles and red triangles represent the results obtained by single  $P_d$  and  $P_v$ , respectively. The black circles and triangles represent the magnitude estimates using  $P_d$  and  $P_v$  by averaging all the available stations, respectively. The dashed line represents the catalog magnitude

Wenchuan earthquake, the estimated magnitude given by the Pd3s method finally stabilized at 5.9 (2.1 magnitude units lower than the catalog magnitude).

In contrast, the APTW method provided the first estimated magnitude of 6.8 just 2.5 s after the first P

wave was triggered (6.8 s after earthquake occurrence). This magnitude estimate remained unchanged until the first three stations were triggered. Incorporating the information from more distant stations, the magnitude underestimation gradually improved and

the final estimated magnitude value stabilized at 7.4 at 22 s after the Wenchuan earthquake.

### 5. Discussion

Empirical relationships of early warning parameters have typically been established in a fixed PTW for magnitude estimation in EEWs. In this study, we investigated the performance of several early warning parameters related to the amplitude, frequency, and energy of seismic P waves in terms of the impact of the time window on the magnitude estimation based on a Chinese strong-motion dataset covering the period 2007–2015. The good performance of the APTW method was demonstrated throughout our study. In this section, we consider several issues concerning the feasibility of future applications and possible improvements for EEWs in other areas.

We discussed the rationality of applying the APTW to establish magnitude-scaling relationships. The APTWs were defined as the time intervals from the P-wave onset to the S-wave arrival; thus, the parameters were calculated over different PTWs based on the hypocentral distances of the triggered stations. As a result of filtering and propagation effects, the P-wave peaks of the displacements of far stations may arrive later; therefore, a longer time window is needed to enable the far stations to better capture the P-wave peaks. Furthermore, using the established relationships, we showed that parameter values with different time windows are randomly distributed in the same earthquake, which indicates that averaging the parameters calculated from different time windows for each earthquake to establish the magnitude-scaling relationships is reasonable.

The amplitude-based parameters ( $P_d^{10\text{km}}$  and  $P_v^{10\text{km}}$ ) are more suitable for applications of the APTW method. The magnitude prediction equations of these parameters have RMSE values of 0.262 and 0.381 magnitude units, respectively. The relationship of the  $P_d$  parameter in the APTWs shows a consistently increasing trend without any saturation effect for  $M$  up to 7, and the underestimation of the  $M_s$  8.0 Wenchuan earthquake was improved compared with the results found when applying the Pd3s method. Unlike the  $P_d$  parameter, the averaged  $P_v^{10\text{km}}$  values

scale with magnitude without saturation for all events. This difference may stem from the different processing steps for the integrated velocity and displacement. Because the integrated velocity waveform rarely shows severe baseline drift, it is not necessary to apply a high-pass filter for the velocity; accordingly, more low-frequency components of large events are retained. Similarly, the energy-based parameter IV2 calculated from the 0.05–10 Hz band-pass-filtered velocity also results in underestimation of the  $M_s$  8.0 Wenchuan earthquake. Although applying APTW improves the correlation between IV2 and magnitude, the process includes more phases (reflected, converted) at larger distances than the direct P wave, producing potentially inconsistent estimations of the energy released during an earthquake. Unlike the amplitude parameters, the frequency-based parameters ( $\tau_p^{\text{max}}$  and  $\tau_c$ ) are less affected by the PTW and are more sensitive to the processing procedures (e.g., high-pass filtering) and data quality.

The values of the coefficient  $A$  in Eq. (2) are lower than those expected from scaling relationships (e.g.,  $A = 1$  for  $P_d$  and  $A = 1.5$  for IV2). A similar phenomenon was found in other studies; for example, Wu and Zhao (2006) used data for 25 regional earthquakes from the Southern California Seismic Network catalog with  $M \geq 4.0$  to obtain the  $P_d$  relationship and obtained a coefficient of magnitude item of 0.63. Comparison of the distribution of  $P_d$  values from our dataset with the relationship of Wu and Zhao (2006) (Supplementary Fig. S2) showed that the relationship of Wu and Zhao (2006) is almost the same as our data distribution. Lancieri et al. (2011) used a dataset containing the  $M_w$  7.8 Tocopilla, Chile, earthquake and its aftershocks to study the magnitude-scaling relationship and found that the coefficient of the magnitude differs for the strong motion and broadband instruments; in the magnitude range of 4–6, the value obtained using the strong-motion data was 0.69, while the value obtained using the broadband data was 1.06, closer to the expected value. The lower coefficients seen in our relationship are partly due to the low-frequency noise that dominates the displacement signal (obtained by a double integration of the recorded accelerations) and may



also be due to the regional characteristics of the P-wave amplitudes.

The original purpose of the APTW was to minimize the underestimation for  $M > 6$  events. The APTW method is more consistent with the characteristics of the rupture processes of earthquakes with different scales. Small events finish rupturing quickly, and for these events, the magnitude estimates are available within a short time following the first P-wave detection with no need to extend PTW. For large events, the expansion of the hypocentral distance allows a longer P-wave signal portion to be captured, providing robust magnitude estimates. Colombelli and Zollo (2015) investigated the time ( $T_{PL}$ ) when the LPDT curve reached the plateau (the time of convergence): the  $T_{PL}$  can be regarded as the peak time of the source time function. They found that the  $T_{PL}$  is approximately 0.5–1 s for events in the range  $M$  4–5, 2–10 s for  $M$  6–7, and approximately 20–25 s for larger earthquakes ( $M$  8–8.5). Thus, to avoid possible underestimation of large events caused by insufficient PTW, the APTW method helps to capture the peak value of P waves within different time windows corresponding to different magnitudes to the greatest extent at each moment after the earthquake occurs.

The APTW method reduces the pull-down effect caused by the subsequent triggering of stations with shorter time windows. During the  $M_w$  7.1 Ridgecrest earthquake that occurred in southern California in 2019, the ShakeAlert EEWS directly averaged the magnitude estimates of all triggering stations at a given moment, such that the magnitude estimates ( $M$  4.1 and  $M$  5.4) of the two stations that received only 0.26 s and 1.03 s of data directly participated in the average of the first four triggered stations, pulling down the average magnitude (5.5) in the initial report, which constituted a serious underestimation of the actual magnitude (Chung et al., 2020). This type of error is greatly reduced when applying the APTW method. As Fig. 11a shows, the far stations are added to the magnitude estimation only when the length of the data reaches the APTW; this ensures that the magnitude estimation is not affected by stations with less available data.

Even though applying the APTW method can reduce the degree of underestimation associated with

large earthquakes, the algorithm starts with a biased estimate for near stations with shorter P-wave time windows, and these biases are not corrected when analyzing data at farther stations. Wang et al. (2020) focused on near-field stations and proposed judging whether an earthquake was large or small based on a pre-established threshold to adopt different magnitude estimation strategies. An appropriate approach to correct the initial bias could be to combine these two methods. For example, the two methods can run in parallel after an earthquake occurs. Then, once the threshold-based method determines that the ongoing earthquake is a large event, the magnitude estimation results can be set to the averaged value of the two approaches. The performance would then be improved by using the result of the threshold-based magnitude estimation method to correct the initial bias of the near-field stations for large events.

## 6. Conclusion

In this study, we proposed a method to establish several magnitude-scaling relationships ( $P_d$ ,  $P_v$ ,  $IV2$ ,  $\tau_p^{\max}$ , and  $\tau_c$ ) by using the APTW and explored a real-time approach that integrates the use of  $P_d$  (the highest correlation with magnitude) and  $P_v$  (having a good performance in predicting large events) using APTWs to estimate the magnitude.

We used an offline simulation to demonstrate the feasibility of the APTW method. The results show that applying the APTW method can provide estimates earlier and that the estimated magnitude is more stable and gradually approaches the catalog magnitude in comparison with a fixed PTW approach. Furthermore, less time is needed to provide an earthquake magnitude estimate, such that a greater lead time is available for the public to take emergency measures. The proposed method provides a new approach to estimate the magnitude for an EEWS, and further testing of data from other regions will be used to further develop the method.

### Acknowledgements

Data for this study are provided by China Strong-Motion Network Centre at the Institute of Engineering Mechanics, China Earthquake Administration. The general drawing tool (Generic Mapping Tools) is used in this paper.

**Author Contributions** YW implemented and applied the methodology and wrote the related text. JS contributed to designing the methodology and revised the article. SL provided important suggestions on the offline test and interpretation of the results. All authors contributed to the redaction and final revision of the manuscript.

### Funding

This research was financially supported by the Scientific Research Fund of the Institute of Engineering Mechanics, China Earthquake Administration (2021C03), the National Natural Science Foundation of China (U2039209, U1534202, 51408564), Natural Science Foundation of Heilongjiang Province (LH2021E119), Spark Program of Earthquake Science (XH22008B), and the National Key Research and Development Program of China (2018YFC1504003).

### Availability of Data and Material

The strong-motion records are not available.

### Code Availability

The code is available by request from the author.

### Declarations

**Conflict of interest** The authors declare no conflicts of interest or competing interests.

**Ethics approval** Not applicable.

**Consent to participate** All authors agree to participate.

**Consent for publication** All authors agree to publish.

**Publisher's Note** Springer Nature remains neutral with regard to jurisdictional claims in published maps and institutional affiliations.

### REFERENCES

- Alcik, H., Ozel, O., Apaydin, N., & Erdik, M. (2009). A study on warning algorithms for Istanbul earthquake early warning system. *Geophysics Research Letters*, *36*, L00B05. <https://doi.org/10.1029/2008GL036659>
- Allen, R. (1982). Automatic phase pickers: Their present use and future prospects. *Bulletin of the Seismological Society of America*, *72*, S225–S242.
- Allen, R. M., Brown, H., Hellweg, M., Khainovski, O., Lombard, P., & Neuhauser, D. (2009). Real-time earthquake detection and hazard assessment by ElarmS across California. *Geophysics Research Letters*, *36*, L00B08. <https://doi.org/10.1029/2008GL036766>
- Allen, R. M., Gasparini, P., Kamigaichi, O., & Böse, M. (2009). The status of earthquake early warning around the world: An introductory overview. *Seismological Research Letters*, *80*, 682–693.
- Allen, R. M., & Kanamori, H. (2003). The potential for earthquake early warning in southern California. *Science*, *300*, 786–789. <https://doi.org/10.1126/science.1080912>
- Allen, R. M., & Melgar, D. (2019). Earthquake early warning: Advances, scientific challenges, and societal needs. *Annual Review of Earth and Planetary Sciences*, *47*, 361–388.
- Allen, R. V. (1978). Automatic earthquake recognition and timing from single traces. *Bulletin of the Seismological Society of America*, *68*, 1521–1532.
- Böse, M., Hauksson, E., Solanki, K., Kanamori, H., & Heaton, T. H. (2009). Real-time testing of the on-site warning algorithm in southern California and its performance during the July 29 2008 Mw5.4 Chino Hills earthquake. *Geophysics Research Letters*, *36*, L00B03.
- Böse, M., Ionescu, C., & Wenzel, F. (2007). Earthquake early warning for Bucharest, Romania: Novel and revised scaling relations. *Geophysical Research Letters*, *34*, L07302. <https://doi.org/10.1029/2007GL029396>
- Chen, D.-Y., Wu, Y.-M., & Chin, T.-L. (2017). An empirical evolutionary magnitude estimation for early warning of earthquakes. *Journal of Asian Earth Sciences*, *135*, 190–197.
- Chung, A. I., Meier, M. A., Andrews, J., Böse, M., Crowell, B. W., McGuire, J. J., & Smith, D. E. (2020). ShakeAlert Earthquake early warning system performance during the 2019 Ridgecrest Earthquake sequence. *Bulletin of the Seismological Society of America*, *110*, 1904–1923. <https://doi.org/10.1785/0120200032>
- Colombelli, S., & Zollo, A. (2015). Fast determination of earthquake magnitude and fault extent from real-time P-wave recordings. *Geophysical Journal International*, *202*, 1158–1163. <https://doi.org/10.1093/gji/ggv217>
- Colombelli, S., Zollo, A., Festa, G., & Kanamori, H. (2012). Early magnitude and potential damage zone estimates for the great Mw 9 Tohoku-Oki earthquake. *Geophysical Research Letters*, *39*, L22306. <https://doi.org/10.1029/2012GL053923>

- Cua, G., Fischer, M., Heaton, T., & Wiemer, S. (2009). Real-time performance of the virtual seismologist earthquake early warning algorithm in Southern California. *Seismological Research Letters*, 80, 740–747.
- Espinosa-Aranda, J. M., Cuellar, A., Garcia, A., Ibarrola, G., Islas, R., Maldonado, S., & Rodriguez, F. H. (2009). Evolution of the Mexico seismic alert system (SASMEX). *Seismological Research Letters*, 80, 694–706. <https://doi.org/10.1785/gssrl.80.5.694>
- Festa, G., Zollo, A., & Lancieri, M. (2008). Earthquake magnitude estimation from early radiated energy. *Geophysical Research Letters*, 35, L22307. <https://doi.org/10.1029/2008GL035576>
- Hsiao, N. C., Wu, Y. M., Shin, T. C., Zhao, L., & Teng, T. L. (2009). Development of earthquake early warning system in Taiwan. *Geophysics Research Letters*, 36, 0002. <https://doi.org/10.1029/2008GL036596>
- Hsu, T. Y., Lin, P. Y., Wang, H. H., Chiang, H. W., Chang, Y. W., et al. (2018). Comparing the performance of the NEEWS earthquake early warning system against the CWB system during the 6 February 2018 Mw 6.2 Hualien earthquake. *Geophysics Research Letters*, 45, 6001–6007.
- Iannaccone, G., Zollo, A., Elia, L., et al. (2010). A prototype system for earthquake early-warning and alert management in southern Italy. *Bulletin of Earthquake Engineering*, 8(5), 1105–1129.
- Kamigaichi, O., Saito, M., Doi, K., Matsumori, T., Tsukada, S. Y., Takeda, K., Shimoyama, T., Nakamura, K., Kiyomoto, M., & Watanabe, Y. (2009). Earthquake early warning in Japan: Warning the general public and future prospects. *Seismology Research Letters*, 80, 717–726.
- Kanamori, H. (2005). Real-time seismology and earthquake damage mitigation. *Annual Review of Earth and Planetary Sciences*, 33, 195–214. <https://doi.org/10.1146/annurev.earth.33.092203.122626>
- Lancieri, M., Fuenzalida, A., Ruiz, S., & Madariaga, R. (2011). Magnitude scaling of early-warning parameters for the Mw 7.8 Tocopilla, Chile, Earthquake and Its Aftershocks. *Bulletin of the Seismological Society of America*, 101(2), 447–463. <https://doi.org/10.1785/0120100045>
- Lomax, A., & Michelini, A. (2009). Mwpd: A duration-amplitude procedure for rapid determination of earthquake magnitude and tsunamigenic potential from P waveforms. *Geophysics Journal International*, 176, 200–214.
- Nakamura, Y. (1988). On the urgent earthquake detection and alarm system (UrEDAS). In *Proceedings of the 9th world conference on earthquake engineering VII* (pp. 673–678).
- Nakamura, Y., & Saita, J. (2007). UrEDAS, the earthquake warning system: Today and tomorrow. In P. Gasparini, G. Manfredi, & J. Zschau (Eds.), *Earthquake early warning systems* (pp. 249–282). Springer.
- Nazeri, S., Shomali, Z. H., Colombelli, S., Elia, L., & Zollo, A. (2017). Magnitude Estimation Based on Integrated Amplitude and Frequency Content of the Initial P Wave in Earthquake Early Warning Applied to Tehran. *Iran. Bulletin of the Seismological Society of America*, 107(3), 1432–1438. <https://doi.org/10.1785/0120160380>
- Peng, C., Ma, Q., Jiang, P., Huang, W., Yang, D., Peng, H., Chen, L., & Yang, J. (2020). Performance of a hybrid demonstration earthquake early warning system in the Sichuan-Yunnan border region. *Seismological Research Letters*, 91, 835–846.
- Peng, H., Wu, Z., Wu, Y.-M., Yu, S., Zhang, D., & Huang, W. (2011). Developing a prototype earthquake early warning system in the Beijing capital region. *Seismological Research Letters*, 82, 394–403.
- Peng, C., Yang, J., Xue, B., Zhu, X., & Chen, Y. (2014). Exploring the feasibility of earthquake early warning using records of the 2008 Wenchuan earthquake and its aftershocks. *Soil Dynamics and Earthquake Engineering*, 57, 86–93. <https://doi.org/10.1016/j.soildyn.2013.11.005>
- Wang, Y., Colombelli, S., Zollo, A., Song, J., & Li, S. (2021). Source parameters of moderate-to-large Chinese earthquakes from the time evolution of p-wave peak displacement on strong motion recordings. *Frontiers in Earth Science*. <https://doi.org/10.3389/feart.2021.616229>
- Wang, Y., Li, S., & Song, J. (2020). Threshold-based evolutionary magnitude estimation for an earthquake early warning system in the Sichuan-Yunnan region, China. *Scientific Reports*, 10, 21055. <https://doi.org/10.1038/s41598-020-78046-2>
- Wu, Y. M., Hsiao, N., Chin, T., Chen, D., Chan, Y., & Wang, K. (2013). Earthquake early warning system in Taiwan. In M. Beer, I. A. Kougioumtzoglou, E. Patelli, & S.-K. Au (Eds.), *Encyclopedia of earthquake engineering*. Berlin: Springer. [https://doi.org/10.1007/978-3-642-36197-5\\_99-1](https://doi.org/10.1007/978-3-642-36197-5_99-1)
- Wu, Y. M., & Kanamori, H. (2005a). Experiment on an onsite early warning method for the Taiwan early warning system. *Bulletin of the Seismological Society of America*, 95, 347–353. <https://doi.org/10.1785/0120040097>
- Wu, Y. M., & Kanamori, H. (2005b). Rapid assessment of damage potential of earthquake in Taiwan from the beginning of the P waves. *Bulletin of the Seismological Society of America*, 95, 1181–1185. <https://doi.org/10.1785/0120040193>
- Wu, Y. M., & Zhao, L. (2006). Magnitude estimation using the first three seconds P-wave amplitude in earthquake early warning. *Geophysical Research Letters*, 33, L16312. <https://doi.org/10.1029/2006GL026871>
- Wu, Y. M., Mittal, H., Huang, T. C., Yang, B. M., Jan, J. C., & Chen, S. K. (2018). Performance of a low-cost earthquake early warning system (P-Alert) and shake map production during the 2018 Mw 6.4 Hualien, Taiwan, Earthquake. *Seismological Research Letters*, 90, 19–29. <https://doi.org/10.1785/0220180170>
- Zhang, H., Jin, X., Wei, Y., Li, J., Kang, L., Wang, S., Huang, L., & Yu, P. (2016). An Earthquake early warning system in Fujian, China. *Bulletin of the Seismological Society of America*, 106, 755–765. <https://doi.org/10.1785/0120150143>
- Ziv, A. (2014). New frequency-based real-time magnitude proxy for earthquake early warning. *Geophysical Research Letters*, 41, 7035–7040.
- Zollo, A., Amoroso, O., Lancieri, M., Wu, Y. M., & Kanamori, H. (2010). A threshold-based earthquake early warning using dense accelerometer networks. *Geophysical Journal International*, 183, 963–974. <https://doi.org/10.1111/j.1365-246X.2010.04765.x>
- Zollo, A., Lancieri, M., & Nielsen, S. (2006). Earthquake magnitude estimation from peak amplitudes of very early seismic signals on strong motion records. *Geophysical Research Letters*, 33, L23312. <https://doi.org/10.1029/2006GL027795>